Theoretical Model of Far-Red-Light-Adapted Photosystem I Reaction Center of Cyanobacterium *Acaryochloris marina* Using Chlorophyll *d* and the Effect of Chlorophyll Exchange

Akihiro Kimura,[*,†] Hirotaka Kitoh-Nishioka,[‡] Toshimichi Aota,[†] Tasuku Hamaguchi,[¶] Koji Yonekura,[¶] Keisuke Kawakami,[¶] Kyoko Shinzawa-Itoh,[§] Natsuko Inoue-Kashino,[§] Kentaro Ifuku,[‖] Eiki Yamashita,[⊥] Yasuhiro Kashino,[§] and Shigeru Itoh[†]

†*Department of Physics, Graduate School of Science, Nagoya University, Furo-cho, Chikusa-ku, Nagoya 464-8602, Japan*
‡*Graduate School of System Informatics, Kobe University, Kobe 657-8501, Japan*
¶*Biostructural Mechanism Laboratory, RIKEN SPring-8 Center, Sayo, Hyogo 679-5148, Japan*
§*Graduate School of Science, University of Hyogo, Ako-gun, Hyogo 678-1297, Japan*
‖*Graduate School of Agriculture, Kyoto University, Kyoto 606-8502, Japan*
⊥*Laboratory of Supramolecular Crystallography, Institute for Protein Research, Osaka University, Suita, Osaka 565-0871, Japan*

E-mail: akimura@tb.phys.nagoya-u.ac.jp
Phone: +81 52 789 2873. Fax: +81 52 789 2873

Abstract

A theoretical model of the far-red-light-adapted photosystem I (PSI) reaction center (RC) complex of a cyanobacterium, *Acaryochloris marina* (AmPSI), was constructed based on the exciton theory and the recently identified molecular structure of AmPSI by Hamaguchi et al (*Nat. commun.*, **2021**, *12*, 1-10.). *A. marina* performs photosynthesis under the visible to far-red light (400-750 nm), which is absorbed by chlorophyll *d* (Chl-*d*). It is in contrast to the situation of all the other oxygenic photosynthesis of cyanobacteria and plants, which contains chlorophyll *a* (Chl-*a*) that absorbs only 400-700 nm visible light. AmPSI contains 70 Chl-*d*, 1 Chl-*d*′, 2 pheophytin *a* (Pheo-*a*), and 12 carotenoids in the currently available structure. A special pair of Chl-*d*/Chl-*d*′ acts as the electron donor (P740) and two Pheo-*a* act as the primary electron acceptor, A_0 as the counterparts of P700 and Chl-*a*, respectively, of Chl-*a*-type PSI's. The exciton Hamiltonian of AmPSI was constructed considering the excitonic coupling strength and site energy shift of individual pigments using the Poisson-TrESP (P-TrESP) and charge density coupling (CDC) methods. The model was constructed to fit the experimentally measured spectra of absorption and circular dichroism (CD) spectra during downhill/uphill excitation energy transfer processes. The constructed theoretical model of AmPSI was further compared with the Chl-*a*-type PSI of *Thermosynechococcus elongatus* (TePSI), which contains only Chl-*a* and Chl-*a*′. The functional properties of AmPSI and TePSI were further examined by the *in silico* exchange of Chl-*d* by Chl-*a* in the models.

INTRODUCTION

Oxygen-evolving photosynthesis in cyanobacteria and plants converts the solar energy into chemical energy and fixes CO_2 to sugars. The absorption of a photon of 400-700 nm visible light excites one of the antenna pigments, and the electronic excitation energy is subsequently transferred to the major pigment chlorophyll *a* (Chl-*a*) and to the special pair of Chl-*a* on the edge and center, respectively, in the photosystem I or II (PSI or PSII) reaction center (RC) complex. The physical properties and spatial arrangements of the pigments in the antenna/RC complexes seem to optimize the efficiencies of excitation energy transfer (EET) and electron transfer (ET).[1] Extensive experimental/theoretical studies of the elementary processes in RCs have revealed optimization mechanisms under diverse natural environments.[2–19]。

PSI[20] and PSII[21] work sequentially in oxygenic photosynthesis.[22] Both PSI and PSII have been known to use Chl-*a* as the major pigment that absorbs 400-700 nm visible light. This is in contrast to the type-I and type-II RCs of anoxygenic photosynthetic bacteria, which use bacteriochlorophylls (BChl) to absorb 400-900-nm visible and far-red light. Therefore, it has been assumed that a higher photon energy of visible light is indispensable for the oxygenic photosynthesis.

A marine cyanobacterium, *Acaryochloris marina* (*A. marina*), and a few other species in this family were found to use a new type of pigment Chl-*d*, that absorbs 400-750-nm light in the oxygenic photosynthesis.[23] Chl-*d* was shown to play an essential role in the photoreaction,[23–26] although *A. marina* contained a small content of Chl-*a* (about 5%) in addition to Chl-*d*. Chl-*d* in *A. marina* can harness far-red light with a photon energy lower than that of visible light, and drives similar photoreactions in both PSI and PSII. Chl-*d* has a Q_y absorption peak at ∼697 nm in methanol, which is ∼30 nm longer than the 665.2 nm Q_y peak of Chl-*a*, and produces ∼80 mV (10%) lower excitation energy. The mechanisms of the photochemical reactions occurring in PSI and PSII of *A. marina* (AmPSI and AmPSII), which produce outputs of chemical energy similar to those of Chl-*a*-based PSI and PSII, respectively, are not yet fully determined. Purified AmPSI had a protein subunit composition similar to that of Chl-*a*-based PSI.[24,26,27] The three-dimensional structure of AmPSI has been clarified recently[28] at a high-resolution of 2.6 Å by cryo-electron microscopy (cryo-EM), as shown in Figure 1. It revealed 70 Chl-*d*, 1 Chl-*d*′, 2 Pheo-*a*, and 12 carotenoids bound to

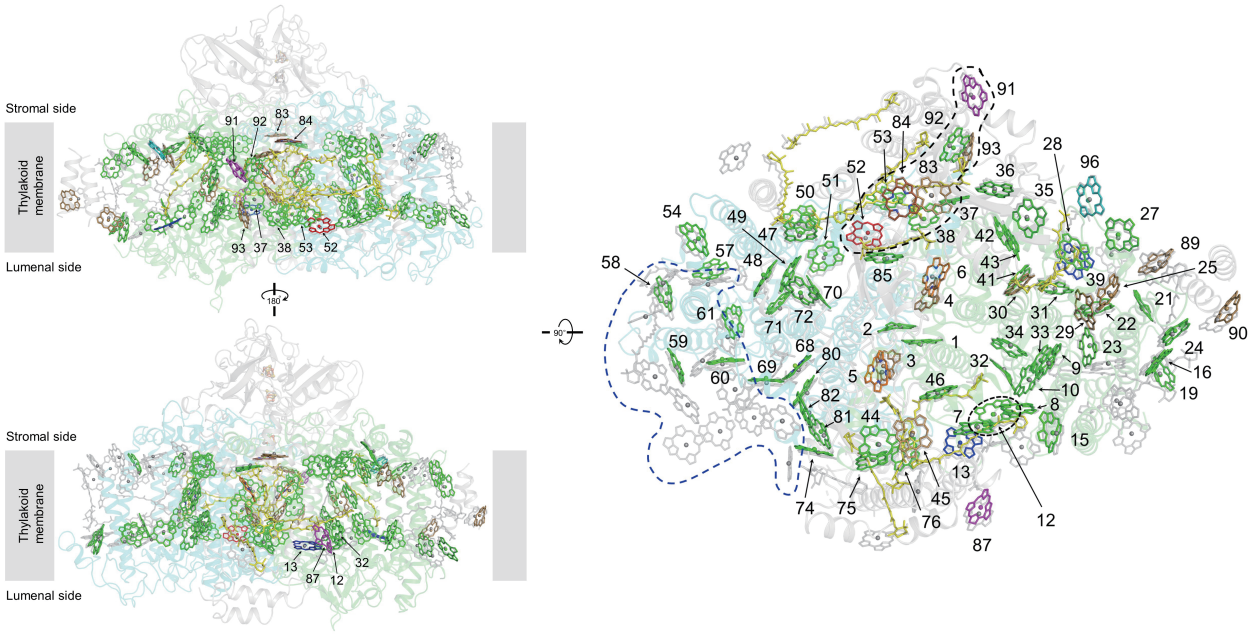

Figure 1: Superposition of pigment arrangements of AmPSI (transparent multicolored) with those of TePSI (transparent grey). Pigment colors indicate the ligand amino acid residues and lipids: green, His; brown, probable water molecule; red, Asp; blue, Gln; magenta, Glu; cyan, phosphatidylglycerol. The dashed black line shows a region where the arrangement of pigments differs from that in TePSI because of the difference in the amino acid residues in the corresponding regions in the subunits Psa27 (PsaI) and PsaL. The dashed blue line shows the disordered region of *A. marina* PsaB. Pigments identified in AmPSI are numbered.

11 protein subunits that are very similar to those in the other PSI as typically seen in the PSI of a cyanobacterium *Thermosynechococcus elongatus* (TePSI) that binds 95 Chl-*a*, 1 Chl-*a*′, and 22 β-caroten. The currently available structures of AmPSI, however, still seem to lack some pigments as described in Discussion section. Therefore, pigment usage in AmPSI is different from that in other type I RCs.

To date, several structures of type I RCs have been determined for the Chl-*a*-using PSI in higher plants,[29,30] green algae,[31,32] red algae,[33] diatoms,[34] cyanobacteria,[13,35–40] including PSI with a low content of Chl-*f*,[13,36,37] and for the type I RCs of BChl-*g*-using anoxygenic bacterium *Heliobacterium modesticaldum*,[41] and BChl-*a*-using green sulfur bacterium *Chlorobaculum tepidum*.[42] All PSI structures, including Chl-*f*-carrying one[13,36,37] except for AmPSI, have Chl-*a* as the major antenna and the electron transfer components as a Chl-*a*/Chl-*a*′ couple, i.e., P700, and Chl-*a* as A_0. The type-I RC of *H. modesticaldum* has BChl-*g* as the major antenna, with BChl-*g*/BChl-*g*′ as P800 and 8^1-OH-Chl-*a* as A_0.[41] The type-I RC of *C. tepidum* has BChl-*a* as the major antenna, with BChl-*a*/BChl-*a*′ as P840 and 8^1-OH-Chl-*a* as A_0.[42] All of them, thus, use Chl-*a*-type A_0. In our recent study of AmPSI structure,[28] P740 was identified as a special pair of Chl-*d*/Chl-*d*′, in contrast to the Chl-*a*/Chl-*a*′ pair (P700) in the Chl-*a*-based PSI.[20] P740 was named after its 740-nm peak of light (oxidation)-induced difference absorption spectrum in analogy to P700.[24] The redox potential of P740 was found to be similar to that reported for P700.[26,27,43] The primary electron acceptor A_0 in AmPSI, however, was identified as pheophytin *a* (Pheo-*a*), in contrast to all the other type-I RCs, which use Chl-*a* type pigments as A_0. P740 gives the longest wavelength absorption band among all the Chl-*d* molecules in AmPSI. It makes a contrast to the majority of Chl-*a*-type PSI, in which a small portion of antenna Chl-*a* molecules that are known as "red-Chls" give absorption peaks at wavelengths longer than 700 nm and work for the "uphill" excitation energy transfer to

P700. The functional mechanism of AmPSI, thus, is interesting.

Recent studies revealed another new type of PSI that uses Chl-f, which shows a Q_y absorption peak at approximately 720-750 nm, to capture far-red light in a variety of cyanobacterial species.[44–46] Chl-f, however, is produced in amounts less than 10% of the total Chl-a in PSI (PSI in *Halomicronema hongdechloris* contains 7 Chl-f and 83 Chl-a[13]) only after growth under far-red light.[35,47] The locations of Chl-fs in PSI of some species, identified by cryo-EM analyses, indicated that Chl-f functions as the peripheral antennae and neither the special pair nor the primary electron acceptor.[13,36] Studies on high-resolution structures[48] and ultrafast spectroscopy[49] have revealed the function of Chl-f in the light-harvesting system in PSI. The roles of Chl-f (and also Chl-d) in PSII are not fully clear yet due to the lack of structural information.[35,50] It has been known that Chl-f is produced only during the growth under far-red light in a wide variety of species of cyanobacteria.[13,36,37,47,49,51] This clearly contrasts with the case of Chl-d in *A. marina*, which consistently produces Chl-d both under white and far-red light as the major pigment in PSI and PSII. The usage of Pheo-a as A_0 in *A. marina* PSI resembles that in type II RCs, namely PSII and bacterial type II RCs, which use Pheo-a and bacteriopheophytin a, respectively, as the primary electron acceptors. The Chl-d-driven PSI system that can use photons of low-energy far-red light is unique. Therefore, the photoreaction mechanism in AmPSI is interesting.

Recent structural studies of the type-I RCs have progressed the theoretical and computational studies of the light-harvesting and electron-transfer processes on the RCs.[13,28–34,36–39,41,42,52,53] Adolphs et al.[8] reproduced the absorption, circular dichroism (CD) and linear dichroism (LD) spectra of TePSI with a high accuracy using the Poisson TrESP (P-TrESP) method and charge density coupling (CDC) method, and identified the spatial distribution of site energy shift at each pigment location, which is essential for the EET process on Chl-a-based PSI of a cyanobacterium TePSI. Using the same strategy, we have constructed the exciton models of natural/modified photosynthetic systems of PSI and *Heliobacterial* RC (hRC) *in silico* and studied the structure–function relationship.[11,16,17] As a result, our exciton model reproduced the absorption, CD, and decay-associated spectra of hRC and revealed that hRC processes a funnel-like distribution of site energy, in contrast to the non-funnel-like one in TePSI.[17]

In this study, we elucidate the light harvesting mechanism of AmPSI based on its structural information and examine its functional and evolutionary differences. The P-TrESP/CDC method was used to obtain the excitonic coupling strength and site energy shift of the exciton Hamiltonian of AmPSI to reproduce the absorption/CD spectra. After the investigation of the physical properties of the exciton Hamiltonian of AmPSI, we calculated the light-induced time-resolved absorption spectra to compare the energy transfer dynamics with the experimental observations.[54,55] The model predicted the short EET time constant of the light-harvesting process and the spatial progression of the reaction well. The model was also used to compare different AmPSI structures, which have been reported by two groups[28,53] with different numbers and locations of the identified Chl-d. To carefully compare the features of AmPSI and TePSI, we re-evaluated the AmPSI structure (PDB code: 7COY) and cryo-EM map of Hamaguchi et al., and compared its Chl-binding sites with those in another AmPSI structure (PDB code: 7DWQ) and TePSI structure. The model also allowed for us to test virtual pigment exchanges on RCs. Using the constructed models, we virtually exchanged all Chl-d in AmPSI including P740 into Chl-a to evaluate the parameters in exciton Hamiltonian and the EET dynamics. The functional (evolutional) differences between the two RCs and the diverse type-I RCs are discussed based on the results.

Method

The exciton Hamiltonian is written by

$$H_{\rm ex}^X = \sum_m E_m^X |m\rangle\langle m| + \sum_{m\neq n} V_{m,n}^X |m\rangle\langle n|. \quad (1)$$

Here, X = Am/Te represents AmPSI/TePSI. $|m\rangle$ represents the localized (first)excited state of the m-th pigment in X. $V_{m,n}^X$ represents the excitonic coupling between the m-th and n-th pigment pairs. Here, E_m^X represents the site energy of the m-th pigment. We used the quantum chemical/electrostatic P-TrESP and CDC methods to calculate $V_{m,n}^X$ and E_m^X, respectively. The calculations were based on the cryo-EM structure (PDB code: 7COY)[28] of AmPSI monomer. Section S1.1 in the Supporting Information explains the preparation of the structure for the calculations in detail. The $V_{m,n}^{\rm Te}$ and $E_m^{\rm Te}$ were reported in the previous papers[16,17] and are used in this study too.

Section S1.2 in Supporting Information describes the P-TrESP method[8,56] to obtain the excitonic coupling strength $V_{m,n}^{\rm X}$ in eq. 1. We derived the transition ESP charges (TrESP) of the heavy atoms of Chl-d, Chl-d', and Pheo-a from time-dependent density functional theory with the CAM-B3LYP functional[57] using locally modified GAMESS 2016.[58] We rescaled the resultant TrESP using the ratio of the experimental to calculated strength of the vacuum transition dipole moment (TDM) for each pigment. We adopted 5.3 Debye for Chl-d and Chl-d' as the strength of the TDMs for scaling based on their experimentally obtained absorption spectra.[59,60] Similarly, we used 4.06 Debye as that of Pheo-a for scaling. For the electrostatic calculations, we used Adaptive Poisson − Boltzmann Solver (APBS) version 1.4.2[61] with an optical dielectric constant $\epsilon_{\rm opt} = 2$. Section S1.2 in Supporting Information provides the details of the P-TrESP calculations.

The CDC method evaluates site energy value E_m^X in eq. 1 as $E_0^m + \Delta E_m^X$, where E_0^m represents the excitation energy of the m-th pigment in vacuum. ΔE_m^X is the site energy shift caused by the pigment–protein interactions in the X RC and is approximated as:

$$\Delta E_m^X = \frac{1}{\epsilon_{\rm eff}} \sum_{J=1}^{K} \sum_{I=1}^{N} \frac{\Delta q_I^{(m)}}{|\mathbf{R}_I^{(m)} - \mathbf{R}_J^{(\rm bg)}|} q_J^{(\rm bg)}, \quad (2)$$

$$\Delta q_I^{(m)} = q_I^{(m)}(1,1) - q_I^{(m)}(0,0), \quad (3)$$

where $q_I^{(m)}(0,0)$ and $q_I^{(m)}(1,1)$ in eq. 3 are the restricted ESP (RESP) charges on the I-th atom of the m-th pigment in the ground and first excited states, respectively. $\mathbf{R}_I^{(m)}$ represents the I-th atomic coordinate of the m-th pigment. $q_J^{(bg)}$ represents the RESP charge of the J-th background atom. We derived $q_I^{(m)}(0,0)$ and $q_I^{(m)}(1,1)$ for Chl-d, Chl-d', and Pheo-a using (TD-)CAM-B3LYP/6-31G(d,p) calculations with the range-separated parameter of $\omega = 0.14$[62] with the Q-CHEM 5.2 program of the suite.[63] $q_J^{(bg)}$ in eq. 2 is derived from the AMBER ff14SB force field[64] for protein and quantum chemical calculations of the cofactors. The details of the CDC calculations are given in Section S1.3 of Supporting Information.

We calculated the exciton states in AmPSI by solving the eigenvalue problem with $H_{ex}^{\rm Am}$ as follows: $H_{\rm ex}^{\rm Am}\Psi_\nu = E_\nu\Psi_\nu$ where E_ν is the eigenvalue of the ν-th exciton state, and its exciton state Ψ_ν is expressed as the following eigenvector: $\Psi_\nu = (C_\nu^1, \cdots, C_\nu^m, \cdots, C_\nu^N)^t$ where C_ν^m denotes the probabilistic amplitude at the m-th site in the ν-th exciton state at the m-th site. The inverse of the participation ratio $N_\nu = (\sum_m |C_\nu^m|^4)^{-1}$ can be used to estimate the pigment number of the delocalization in the exciton state ν.

The absorption, CD, and transient absorption difference spectra are, expressed as follows, respec-

tively:

$$A(E) \propto E \sum_{\nu=1}^{N} |\boldsymbol{\mu}_\nu|^2 D_\nu(E), \tag{4}$$

$$\mathrm{CD}(E) \propto E \sum_{\nu=1}^{N} \sum_{m>n}^{N} C_\nu^m C_\nu^n \boldsymbol{r}_{mn} \cdot (\boldsymbol{\mu}_m \times \boldsymbol{\mu}_n) D_\nu(E), \tag{5}$$

$$\Delta A(E,t) \propto -E \sum_{\nu} |\boldsymbol{\mu}_\nu|^2 \rho_\nu(t) D_\nu(E). \tag{6}$$

In eq. 6, we neglected the bleaching of absorption bands of ground state and the appearance of excited state bands to highlight the dynamics of excitation process, although the experimentally available transient absorption spectra include the bleaching of ground state, fluorescence emission, and the appearance of absorption due to the transient excited state. The TDM $\boldsymbol{\mu}_\nu$ for each exciton state ν in eqs. 4, 5 and 6 is expressed as a linear combination of the transition dipole moments $\boldsymbol{\mu}_m$ of the m-th pigment using site representation as follows: $\boldsymbol{\mu}_\nu = \sum_{m=1}^{N} C_\nu^m \boldsymbol{\mu}_m$. The distance vector, $\boldsymbol{r}_{mn}$, is obtained from the position of the Mg atom in n-th pigment to that of m-th pigment. We define the density of the exciton state $D_\nu(E)$ by assuming the Markovian limit as:

$$D_\nu(E) = \frac{1}{2\pi} \int dE' \frac{e^{-E'^2/\sigma^2}}{\sqrt{\pi\sigma^2}} \frac{\hbar k_\nu^R}{(E + E' - E_\nu)^2 + \hbar^2 k_\nu^{R2}/4}, \tag{7}$$

where k_ν^R is the lifetime of ν-th exciton state defined as $k_\nu^R = \sum_{\mu \neq \nu} k_{\mu\nu}^R$. $D_\nu(E)$ in eq. 7 is averaged over the static disorder weighted by the Gaussian distribution function of dispersion σ. We assume that the probability of the ν-th exciton state satisfies the master equation based on the Redfield equation as follows: $\dot{\rho}_\mu(t) = \sum_\nu k_{\mu\nu}^R \rho_\nu(t)$. The Redfield rate formula[65] is expressed as:

$$\begin{aligned} k_{\mu\nu}^R =& 2\pi \sum_{m=1}^{N} \Omega_{\nu\mu}^2 (C_\mu^m C_\nu^m)^2 \\ & \times [J(\Omega_{\nu\mu})(n(\Omega_{\nu\mu}) + 1) + J(\Omega_{\mu\nu}) n(\Omega_{\mu\nu})], \end{aligned} \tag{8}$$

where $J(\Omega_{\nu\mu})$ in eq. 8 is the density of the states with exciton-phonon interactions, $n(\Omega_{\nu\mu})$ is the Bose–Einstein distribution function, and $\Omega_{\nu\mu}$ is defined as $(E_\nu - E_\mu)/\hbar$.

An analysis was performed for the structure of the AmPSI monomer (7COY), which contains 73 pigments in total. The TDMs of all Chl-d and Chl-d' were set as 5.3 Debye and that of Pheo-a as 4.06 Debye. Note that the P-TrESP method is not applicable to short-range excitonic coupling in P740.[16] Therefore, in this study we simply set the coupling to 168.2 cm^{-1}. The value was scaled from the excitonic coupling strength in P800 of the hRC, considering the ratio between the TDMs of Chl-d and BChl-g. The effective dielectric constant was set to $\epsilon_{\mathrm{eff}} = 1.4$ in the evaluation of the site energy shift. The site energies of Chl-d (Chl-d') and Pheo-a in a vacuum were set to $E_0^{\mathrm{Chl}-d}$ = 700 nm and $E_0^{\mathrm{Pheo}-a}$ = 666 nm respectively, to reproduce the peak positions and widths of the experimental absorption/CD spectra. We use the function $J(\omega)$ in eq. 8 as follows:

$$J(\omega) = \sum_{n=1,2} \frac{s_n}{7!2\omega_n^4} \omega^3 e^{-(\omega/\omega_n)^{1/2}}, \tag{9}$$

where the parameters are defined as $s_1 = 0.8$, $s_2 = 0.5$, $\hbar\omega_1 = 0.069$ meV, and $\hbar\omega_2 = 0.24$ meV.[66] The width σ, which represents the static disorder, was set at 160 cm^{-1} at 5 K and 170 cm^{-1} at room temperature to reproduce the experimental spectra.

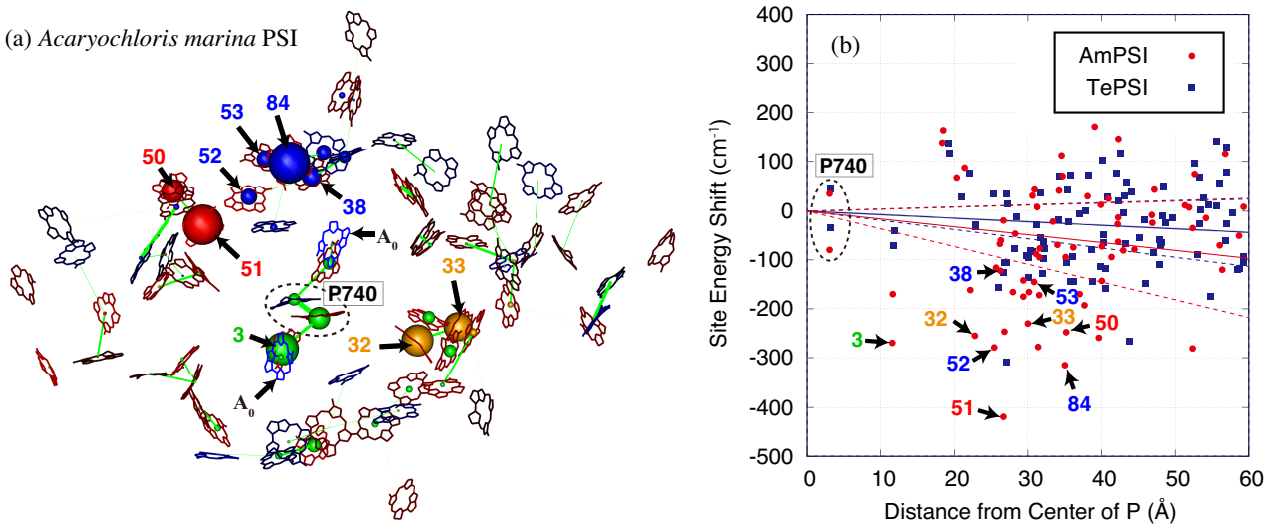

Figure 2: (a) Pigment arrangement in AmPSI. The green lines represent the excitonic coupling strength $V_{m,n}^{\mathrm{Am}}$ between the pigments. The red/blue color of the pigment represents the negative/positive site energy shift ΔE_m^{Am} of each pigment. The size of the Mg spheres represents the extent of the distribution of the excitation energy in the lowest (red), 2nd (orange), 3rd (green), and 4th (blue) exciton states. (b) Dependencies of site energy shifts on distance from the center of P740 in AmPSI (red circles) and P700 in TePSI (blue squares).

RESULTS

Figure 2a shows the sign and value of site energy shift ΔE_m^{Am} for each pigment in AmPSI calculated by eq. 2, expressed in red (negative) and blue (positive). The squared value of the excitonic coupling strength, $|V_{m,n}^{\mathrm{Am}}|^2$, in each pigment pair is indicated by the width of the green line. Each line corresponds to the pair with the maximum absolute value of excitonic coupling strength between the selected pigment and the others. The number of pigments in Figure 2 is given after numbering, according to Hamaguchi et al.[28] The values of site energy shift ΔE_m^{Am} are are listed in Table 1. The values of excitonic coupling strength $V_{m,n}^{\mathrm{Am}}$ are listed in Supporting Information.

The distributions of the excited states are shown in Figure 2a by the sphere size on central Mg atom of each pigment for the lowest (red), 2nd (orange), 3rd (green), and 4th (blue) exciton states. The distributions of excitation energy on all the 73 exciton states are shown in the movie in Supporting Information. In the lowest exciton state, the excitation energy was mostly located on the 50th and 51st Chl-*d*. The site energy shift of the 51st Chl-*d*, in particular, is negatively shifted as $\Delta E_{51}^{\mathrm{Am}} = -420$ cm^{-1}; thus, it should be the most excited pigment in the lowest exciton state. In the second and third exciton states, the 3rd, 32nd, 33rd Chl-*d*, and special pair P740 were likely to be in the excited states. In the 4th and 5th exciton states, the 38th, 52nd, 53rd, and 84th Chl-*d* were likely to be in the excited states. The large negative values of the site energy shift in the model indicate high excitation distributions of the excitation on these pigments in the lower exciton states.

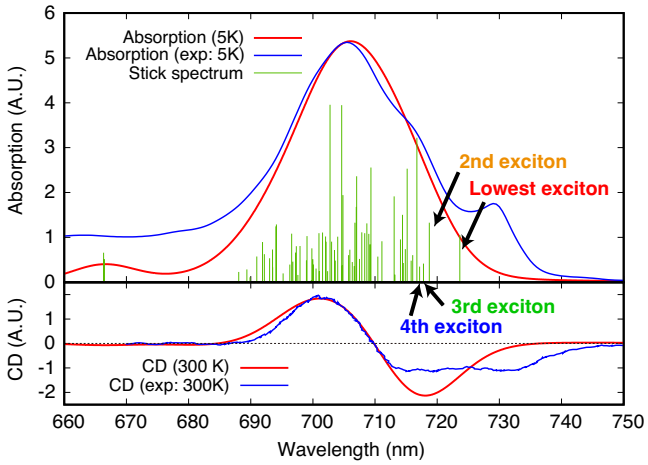

Figure 3: Absorption spectrum measured at 5K, and CD spectrum at room temperature of AmPSI where we set artificial parameters $E_0^{\mathrm{Chl}-d}$, $E_0^{\mathrm{Pheo}-a}$, and ϵ_{eff} to 700 nm, 666 nm, and 1.4. The static disorder σ is set to 160 cm^{-1} at 5 K and σ = 170 cm^{-1} at 300 K. Theoretically calculated line spectrum, absorption spectrum and CD spectrum are also shown.

Figure 3 shows the numerical calculations of the absorption spectrum by eq. 4 of AmPSI at 5 K and the CD spectrum at room temperature by eq. 5 together with the experimentally measured ones.[67] The artificial parameters ($E_0, \epsilon_{\mathrm{eff}}$, and σ) were adjusted to reproduce the experimental peak and shoulder of the absorption/CD spectra at approximately 700 nm. The absorption strength at longer wavelengths, for example, 730 nm, could not be reproduced well, as experienced in the analysis of TePSI for the reproduction of Chl-*a* longwavelength bands.[8] The negative CD values, calculated at approximately 720 nm, are larger than the measured values. A proper correction of the parameters in exciton Hamiltonian, which contributes to these exciton states should lead to better simulation of the absorption and CD spectra in the future.

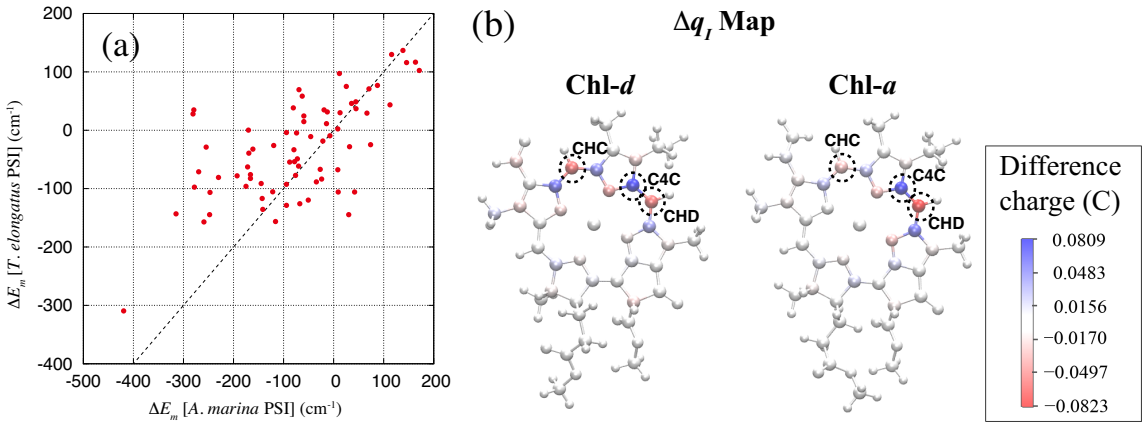

Figure 4: (a): Relation between the values of site energy shifts ΔE_m^X for AmPSI and TePSI. (b) Distribution of ESP difference charges Δq_I in Chl-*d* and Chl-*a*, calculated by the CDC method.

The correlation between the values of site energy shift ΔE_m^X for AmPSI and TePSI obtained using the CDC method of eq. 2 is shown in Figure 4a to understand their functional/evolutional differences. Each pigment in AmPSI located at its counterpart position in TePSI is defined as shown in Table 1. Positive correlation was found between the pigments in AmPSI and TePSI regardless of their different molecular arrangement. It is contrary to the weak correlation detected between hRC and TePSI.[17]

Table 1: Site energy shift values ΔE_m^X (cm^{-1}) for AmPSI and TePSI. Asterisks on pigment number indicate the seven Chl-d sites newly identified in Ref. 53. " — " represents "not applicable".

Pig#	ΔE_m^{Am}	ΔE_m^{Te}	AmPSI	TePSI	Pig#	ΔE_m^{Am}	ΔE_m^{Te}	AmPSI	TePSI
1	-111.125	-50.088	A3101	A1011	49	11.745	-101.603	B3005	B1203
2	49.771	68.487	B3003	B1021	**50**	-346.897	-216.474	B3006	B1204
3	-377.329	-106.471	B3002	B1012	**51**	-587.381	-464.225	B3007	B1205
4	-237.438	-58.755	A3103	A1022	**52**	-390.908	52.571	B3008	B1206
5	228.728	175.298	A3102	A1013	**53**	-202.677	-136.638	B3009	B1207
6	193.427	204.819	B3004	B1023	54	11.406	3.619	B3010	B1208
7	98.584	106.683	A3104	A1101	55	—	118.662	—	B1209
8	-238.341	0.45	A3105	A1102	56	—	-87.017	—	B1210
9	-269.907	-117.243	A3106	A1103	57	62.063	73.312	B3011	B1211
10	-240.858	-94.658	A3107	A1104	58	-97.97	-91.873	B3012	B1212
*11	—	-31.212	—	A1105	59	-393.441	42.191	B3013	B1213
12	-162.259	-234.19	A3108	A1106	60	-17.971	46.718	B3014	B1214
13	-83.784	22.504	A3109	A1107	61	-363.301	-235.876	B3015	B1215
*14	—	103.249	—	A1108	62	—	-163.933	—	B1216
15	-10.448	-14.628	A3110	A1109	63	—	-138.155	—	B1217
16	161.984	194.898	A3111	A1110	64	—	-177.299	—	B1218
*17	—	-107.422	—	A1111	65	—	-263.277	—	B1219
*18	—	-35.38	—	A1112	66	—	-222.658	—	B1220
19	-167.644	-38.749	A3112	A1113	67	—	-398.455	—	B1221
20	—	18.597	—	A1114	68	-232.483	-114.223	B3016	B1222
21	-48.388	-132.987	A3113	A1115	69	-30.007	-27.323	B3017	B1223
22	204.148	174.016	A3114	A1116	70	-225.76	-48.456	B3018	B1224
23	-199.906	-175.662	A3115	A1117	71	-198.102	-203.359	B3032	B1225
24	12.443	-158.268	A3116	A1118	72	-132.401	-192.838	B3019	B1226
25	-33.596	-125.901	A3117	A1119	73	—	32.816	—	B1227
*26	—	-4.051	—	A1120	74	239.695	153.598	B3020	B1228
27	103.484	-37.3	A3118	A1121	75	44.717	-42.309	F 201	B1229
28	-109.404	-80.328	A3140	A1122	76	-345.495	-159.319	B3021	B1230
29	-37.512	-100.495	A3119	A1123	77	—	-168.576	—	B1231
30	-64.293	-16.144	A3120	A1124	78	—	-96.274	—	B1232
31	-96.516	104.46	A3121	A1125	79	—	83.511	—	B1233
32	-356.68	-42.876	A3141	A1126	80	-94.34	-189.108	B3022	B1234
33	-322.369	-121.215	A3122	A1127	81	-245.008	-144.151	B3023	B1235
34	-389.418	-145.767	A3142	A1128	82	-123.237	-82.024	B3024	B1236
35	35.461	113.023	A3123	A1129	83	157.095	65.264	A3133	A1237
36	17.876	44.673	A3124	A1130	**84**	-441.033	-214.719	B3025	B1238
37	62.368	55.678	A3125	A1131	85	93.596	44.248	B3026	B1239
38	-170.406	-158.117	A3126	A1132	*86	—	108.035	—	F1301
39	-101.013	-73.395	A3127	A1133	87	-131.424	-5.509	H 101	J1302
40	—	-20.692	—	A1134	88	—	-27.693	—	B1303
41	-26.739	52.458	A3128	A1135	89	-70.488	-179.221	A3146	K1401
42	-232.392	-123.931	A3129	A1136	90	-82.908	36.978	I 101	A1402
43	-106.629	-115.656	A3130	A1137	91	-19.659	16.922	J 202	L1501
44	58.645	-158.916	A3131	A1138	92	-112.595	57.841	J 203	L1502
45	-131.877	-138.776	A3132	A1139	93	-87.674	87.733	J 204	L1503
46	122.362	115.005	A3143	A1140	*94	—	212.749	—	M1601
47	-103.555	-6.787	B3030	B1201	95	—	-97.361	—	X1701
48	42.624	-216.98	B3031	B1202	96	16.11	145.564	A3134	A1801

In Figure 2b, the value of the negative or positive site energy shifts ΔE_m^X for each pigment was plotted against the distance from the center of a special pair, shown as a red circle or a blue square in AmPSI and TePSI, respectively. The distance distributions of the site energy shift are compared between AmPSI and TePSI in Figure 2b. By fitting a straight line to the scattered points, it can be seen that the distribution of the site energy shift is not funnel-like in AmPSI. This is similar to the case of TePSI, although the gradient was larger in AmPSI. Some Chl-*d* in AmPSI had larger negative values of site energy shifts compared to Chl-*a* at the corresponding locations in TePSI. These Chl-*d*s point outside the standard deviation range of the fitting line in Figure 2. The spatial distributions of excitation energy in some lower exciton states of AmPSI resemble those of TePSI. This is due to the positive correlation between the site energy shift values in AmPSI and TePSI. However, the present models do not reproduce the exciton states, responsible for the 'long wavelength shifted' states at 730 nm in AmPSI and the Red-Chl-*a* states in TePSI.

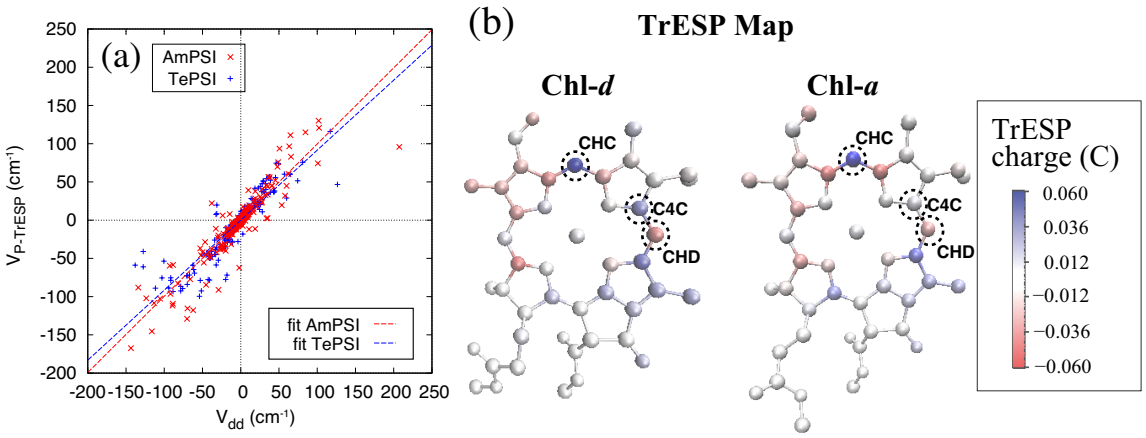

Figure 5: (a): Correlation between the values of excitonic coupling between pigments on AmPSI, calculated by P-TrESP and d-d approximation methods. (b) Distribution of transition ESP charges in Chl-*d* and Chl-*a*

Figure 5 shows the correlation between the excitonic coupling strength values $V_{m,n}^{\mathrm{Am}}$ numerically calculated by the P-TrESP method of eq. S3 and the simpler dipole-dipole (d-d) approximation method in AmPSI. The fitting lines to the distribution show the better correlation between the excitonic coupling strength and the d-d approximation in AmPSI than that in TePSI. Correlation between the excitonic coupling strengths in AmPSI calculated by TrESP method and P-TrESP method is analyzed. As shown in Figure S1, the dielectric screening effect, which is almost equal to inverse of ϵ_{eff}, was estimated as a factor of 0.714. Therefore, the simple d-d approximation method also gives rather reliable exciton coupling strength for Chl-*d* molecules in AmPSI compared to the case of Chl-*a* molecules in TePSI.

The inverse of the participation ratio of the exciton states in AmPSI was also calculated (Figure S2 in Supporting Information). The largest delocalized pigment size in all the excited states amounted to 16 % (12 pigments) of the whole system in AmPSI. The number is nearly equal to that of 16 found in hRC and is smaller than 25 found in TePSI.[17]

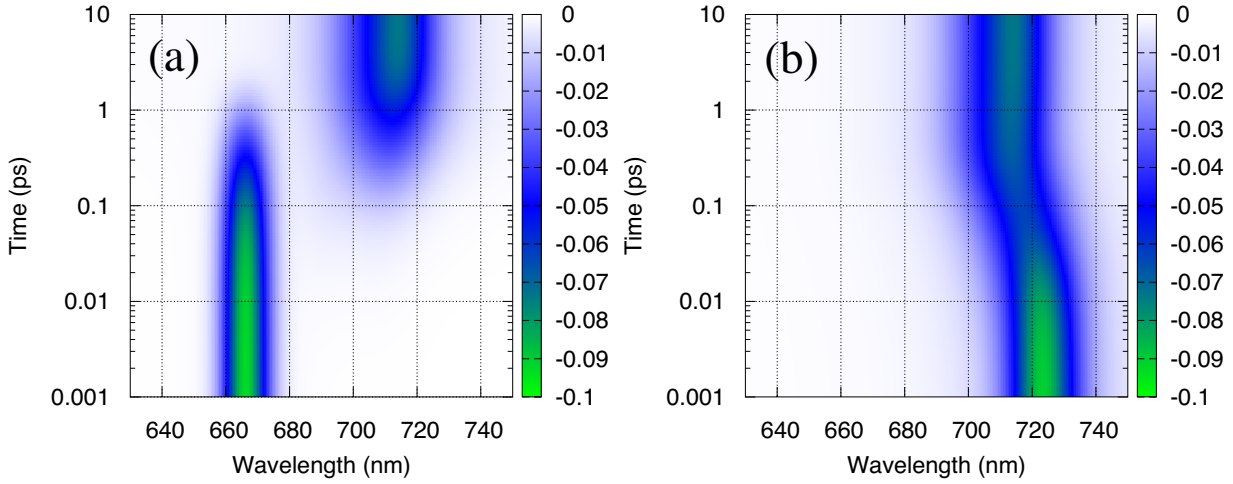

Figure 6: Estimated transient absorption change $\Delta A(\lambda, t)$ of AmPSI after 630 nm (a) and 740 nm (b) laser pulse excitation.

Transient absorption spectra induced by 630 and 740 nm laser pulses were recorded for AmPSI.[54,55] We calculated these spectra with eq. 6, as shown in Figure 6. The calculation indicated the spectra after the 630 nm excitation, as shown in Figure 6a. Pheo-*a* is excited first, giving rise to the absorption change around 670 nm, as observed experimentally (although the presence of Pheo-*a* in AmPSI was not known when the experiment was performed).[54,55] The excitation energy transfer from the excited Pheo-*a* to Chl-*d* in the lower exciton states at approximately 710 nm was reproduced on the time scale of about 1 ps, producing a rather long-lived excited state at 710 nm, as seen in the measurement.

DISCUSSION

Optical properties and EET mechanism in AmPSI calculated by the exciton model

We constructed an exciton model of AmPSI, based on structure-based theoretical calculations, using the P-TrESP/CDC methods. AmPSI is a unique RC. It uses Chl-*d* as the major antenna pigment and as the special pair P740, and uses two Pheo-*a* as the electron acceptor A_0 to perform photoreactions using far-red light. It demonstrates a clear contrast with all the other PSI using Chl-*a* as the major antenna, the special pair P700, and A_0. Therefore, the functional mechanism of the Chl-*d*-using AmPSI was tested by constructing the theoretical model in this study. The model reproduced the observed spectral bands of absorption/CD spectra around the peaks and shoulders, as shown in Figure 3. The exciton model assuming the constant site energy values (703 nm) for all the pigments including Pheo-*a* gave the absorption line-spectrum plotted in Figure S3. Although the model assuming the extremely large disorder at $\sigma = 250$ cm^{-1} gave a bandwidth which is similar to the experimental one as shown in Figure S3, the calculated line spectra somewhat deviated from those of Figure 3. The constant site energy model with the extremely large disorder, however, did not fit the peak positions and bandwidths of the experimental CD spectrum correctly. Hence, the proper estimations of excitonic coupling strengths and the site energy shifts are important for the correct reproductions of the absorption/CD spectra. The model also reproduced the transient spectral changes during the ultrafast EET process measured after the pulse laser excitation of AmPSI, as shown in Figure 6. The model calculation indicated the appearance of a quasi-stationary state at approximately 1 ps at around 710 nm in the downhill EET. The predicted 710 nm peak

interprets the quasi-stationary state measured at approximately 730 nm. It should be also noticed that the analysis of exciton dynamics in AmPSI would be more appropriate to use a combination of Redfield and generalized Förster theory in order to avoid an artificial delocalization of excited states due to the dynamical disorder.[6,8] By contrast, the current model could not reproduce the "long wavelength Chl-*d*" bands at around 730 nm detected either in the absorption or the CD spectra, and the excited state of special pair P740. The ability of the model to correctly reproduce the long wavelength bands should be increased in refined models in the future.

It was concluded that the optical properties and exciton dynamics of the Chl-*d*-based AmPSI system can be reproduced by the current theoretical model, as previously reported for TePSI.[8] The two types of models qualitatively reproduced the exciton states and EET dynamics of AmPSI and TePSI rather well, except for the longer wavelength bands. The exciton Hamiltonians and light-harvesting mechanisms of AmPSI and TePSI are further examined below.

Difficulty in the reproduction of the long wavelength side absorption bands

The current exciton model of AmPSI poorly reproduces the absorption band at approximately 730 nm, as shown in Figure 3. The situation resembles the case reported in TePSI, in which reproduction of the "red-Chl-*a*" bands with peak wavelengths longer than that of P700 was attempted by the P-TrESP/CDC methods. Almost all the longer wavelength Chl-*d* peaks in AmPSI are at wavelengths shorter than the 740-nm peak of P740, as shown in Figure 3. It seems necessary of either application of a more accurate quantum chemical calculation method to modify the exciton model, or better structural considerations of AmPSI. The calculated absorption spectra showed intensities that were higher and lower than those in the measured spectrum at about 710 and 730 nm, respectively. Therefore, if we can shift the site energy values of the pigments, which contribute to the extra intensities at around 710 nm in the model, it will better reproduce the bands above 720 nm in the absorption and CD spectra of AmPSI. It is also noted that 50th and 51st Chl-*d*s are excited in the lowest exciton state, and that Chl-*d*/Chl-*d*′ in the special pair P740 are excited in the 2nd and 3rd lowest exciton states, as shown in the Supporting Information movie. However, these exciton states do not contribute to the absorption intensity at 730-740 nm in the model, where absorption change at about 740 nm is shown to be induced by the P740 oxidation.[24,27] Therefore, a more advanced quantum chemical calculation method, as well as the additional information for the location/exciton state of individual pigments, especially for special pair of Chl-*d*/Chl-*d*′, is required for the calculations of the exciton states of the electron transfer components in AmPSI as treated elsewhere. The electron exchange interaction between the closely contacted pigments such as the special pair pigments will give significant contributions to the value of site energy shifts and excitonic couplings and will contribute to the future better calculation of the red-shifted transitions that were not reproduced well in the current model. Although the static disorder was considered empirically in this study, local fluctuations of the protein scaffold will also affect the CDC/P-TrESP calculations. These effects might be more critical for the case of pigment-exchange calculations, where the protein structure would most likely relax somehow to accommodate such fluctuations.

Evaluation of the structures proposed by the two recent Cryo-EM studies

Following the report on the 2.6 Å-structure of AmPSI by Hamaguchi et al.,[28] which was used in this study, Xu et al. reported the AmPSI structure with 3.3 Å resolution by cryo-EM analysis[53] (PDB code: 7DWQ). The 3.3 Å-structure included 1 Chl-*d*′, 76 Chl-*d* (more Chl-*d* compared to the

2.6 Å-structure), 2 Pheo-a. Thus, we calculated a difference map, the F_o - F_c difference map, using the cryo-EM map (two-half maps) of Hamaguchi et al.[28] and carefully re-identified Chls and their binding sites. This procedure added 7 more Chl-d positions to the former 2.6 Å-structure, as shown in Figure S4, although some more Chl-d molecules seem to be still missing even in this analysis. It is, however, difficult to calculate site energy shift and excitonic coupling for these 7 Chl-d molecules by CDC/P-TrEPS methods because of the lack of information for the precise structure of protein moiety due to the low resolutions.

We then estimated the values of site energy shifts for the newly identified seven Chl-d, which are comparable to the Chl-a molecules situated at corresponding positions in TePSI. Asterisks have been added to their pigment numbers in Table 1. The newly identified Chl-d sites have rather low absolute values of the site energy shift so that they do not seem to correspond to the sites of long wavelength Chl-d or the red-Chl-a sites in TePSI. On the other hand, the large negative site energy shifts of the 62nd-67th Chl-a in TePSI distribute their excitations in the 2nd exciton state in TePSI, as shown in Figure S5b. However, these Chl-a sites have no counterparts among the new Chl-d sites. Hence, the exciton Hamiltonian that includes the excited states of the newly identified 7 Chl-d should increase the absorption intensity around the 700-nm peak, and do not seem to contribute to the absorption band at 730 nm in AmPSI at present.

It is interesting that both the two 2.6 and 3.3 Å cryo-EM structures indicated A_0 as Pheo-a because they lacked the Mg^{2+}-derived map density. The conclusion was also supported by the chemical analysis of the extracted pigments in the report of 2.6 Å structure.[28] It has long been known that the chemical identities of the primary electron acceptor A_0 in type-I RCs (PSI, heliobacterial, and green sulfur bacterial RCs) are Chl-a species until the determination in the AmPSI structure.[20,41,42] The ET mechanism in AmPSI should be different from the other type-I RCs. Thus, it is necessary to analyze the ET mechanism in AmPSI that uses Pheo-a instead of Chl-a as A_0. Theoretical estimations of the values of the oxidation-reduction potential of the special pair (P740), A_0 (Pheo-a), and A_1 (phylloquinone) are currently underway based on the present model.

In all the other PSI, β-carotene, but not α-carotene, is used. It is another mystery in the EET mechanism of AmPSI since the first report of PSI purification by Hu et al.,[24] who chemically identified α-carotene in purified AmPSI. Hamaguchi et al. analyzed the arrangement of identified carotenoids together with the protein structure around them in AmPSI, focusing particularly on the ring (α or ϵ) of Car4007 and the 38th, 52nd, and 53rd Chl-d because the protein structure surrounding them are slightly different from the corresponding one in TePSI. Xu et al. did not describe the details of the structural identification of α-carotene (different β- and ϵ-rings of carotenoids). The features of the EET around Car4007 and Chl-d molecules in AmPSI are also very interesting.

Car4007 has been shown to contribute significantly to the site energy shift of the 53rd Chl-d, $\Delta E_{53}^{\mathrm{Am}}$, by the component decomposition analysis in this study. The 53rd Chl-d participates in the 4th and 5th lowest exciton states. It is also found that Car4007 contributes to the site energy shift of 53rd Chl-d in the top 20 of all 2185 molecules in the component decomposition analysis. The top 20 molecules are located on the His95 side, as shown in Figure S6 in Supporting Information. There are a few components (amino acid residues) on the other side, except for Car4007, which contributes to the site energy shift of the 53rd Chl-d. This high contribution may be due to the steric hindrance caused by this carotenoid, which has an electrostatic interaction with the 53rd Chl-d weaker than His95. The study of the EET dynamics from carotenoids to Chl-d in lower exciton states may further reveal the functional roles of carotenoids in AmPSI and TePSI in future.

Analysis of "Chl-*a*-containing AmPSI" produced by the virtual *in-silico* pigment exchange

The excitonic coupling strengths of Chl-*d* molecules in AmPSI, calculated using the P-TrESP method of eq. S3, show a positive correlation with those calculated using the simple d-d approximation method, as shown in Figure 5a. It is slightly different from the observation in TePSI, indicating that the distribution of the TrESP charge in Chl-*d* can be expressed well by the transition dipole in the Q_y direction in contrast to that in Chl-*a*. Figure 5b compares the distributions of transition ESP charges in Chl-*d* and Chl-*a*, where Tables S4 – S6 in the Supporting Information list the scaled TrESP charges for Chl-*d*, Chl-*d*′, and Pheo-*a*, respectively. The charge on carbon C4C in Chl-*d* is clearly more positive than that in Chl-*a*. This indicates that the excitonic coupling between Chl-*a* molecules is affected more strongly by the charge distributions in the Q_x direction compared to that between Chl-*d* molecules. It interprets that even the approximation by the simple d-d method yielded reasonable results in AmPSI. The distributions of ESP difference charges in Chl-*d* and Chl-*a* structures are also shown in Figure 4b, where Tables S1 – S3 in the Supporting Information list the Δq_I for Chl-*d*, Chl-*d*′, and Pheo-*a*, respectively. The charge on the carbon CHC in Chl-*d* is more negative than that in Chl-*a* due to the more symmetrical charge distribution along the Q_y axis. This indicates that the site energy shifts of Chl-*a* molecules are more affected by the charge distributions along the Q_y direction than those of Chl-*d* molecules. This induces different site energy shifts between Chl-*a* and Chl-*d*, even in similar protein environments of AmPSI and TePSI, as shown in Figure 2b.

We then studied the effects of virtual exchange of Chl-*d* by Chl-*a* on the excitonic coupling strength, site energy shift, and exciton dynamics in AmPSI. We replaced the formyl group on Chl-*d* with a vinyl group first, and then the two carbons and a hydrogen in the vinyl group in the resultant Chl-*a* were structurally optimized. After the pigment exchange and structure optimization, all the parameters in the exciton Hamiltonian of eq. 1 were numerically recalculated using the P-TrESP/CDC methods. The absolute values of the excitonic coupling strength and site energy shift obtained after the pigment exchange were not significantly different, indicating that each Chl-*d* in AmPSI can be changed to Chl-*a* *in silico* without significant steric hindrance. We then compared the Hamiltonian of Chl-*a* introduced AmPSI, designated as AmPSI(Chl-*a*) hereafter, with that of native AmPSI or native TePSI.

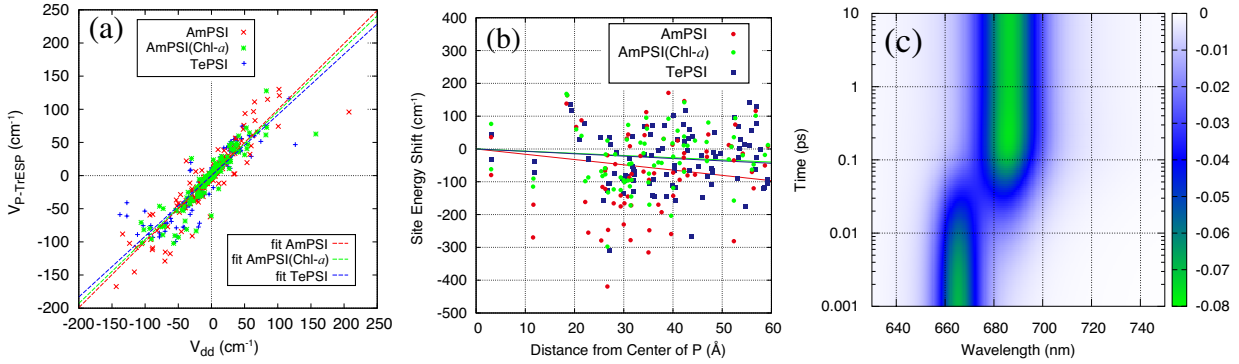

Figure 7: (a): Correlation between the values of excitonic coupling strength calculated by P-TrESP and d-d approximation methods in TePSI, AmPSI, and AmPSI(Chl-*a*). (b) Relationship between the site energy shift and the distance from the center of the special pair in TePSI, AmPSI, and AmPSI(Chl-*a*). (c) Transient difference absorption spectrum of AmPSI(Chl-*a*).

The correlation between the values of the excitonic coupling strength calculated by the d-d approximation and the P-TrESP methods in the Chl-*d*- and Chl-*a*-containing AmPSI's is evaluated,

as shown in Figure 7a. The correlations with the fitting line were 0.964, 0.996, and 0.915 for AmPSI(Chl-*a*), native Chl-*d*-containing AmPSI, and native Chl-*a*-containing TePSI, respectively. The high correlations indicate that Chl-*a* can replace Chl-*d* in AmPSI without significant problems on the functional properties and that the calculation by the d-d approximation method was less reliable for the Chl-*a* containing AmPSI compared to that for (native) Chl-*d* containing AmPSI. This is due to the different distributions of the transition ESP charges on Chl-*a* and Chl-*d*. The different physical properties of the pigments result in different excitonic couplings. The virtually produced "Chl-*a*-introduced AmPSI" thus produced the physical property closer to the native (Chl-*a* containing) TePSI than to the "native Chl-*d*-containing AmPSI"

Figure 7b shows the relation between the site energy shifts and the distance from the special pair in the TePSI, AmPSI, and AmPSI(Chl-*a*). Although some pigments showed significantly different values or inverted signs of site energy shift, suggesting variations in interactions with their protein environments, the whole relationship is almost similar to that of native TePSI. The correlation between the site energy shifts in AmPSI(Chl-*d*) and AmPSI(Chl-*a*) calculated by CDC method was also analyzed. As shown in Figure S7, there is a positive correlation between them. It indicated positive correlations between the site energies of individual pigments in AmPSI(Chl-*a*) and their counterparts in TePSI. It is, therefore, concluded that the Chl-*d* to Chl-*a* exchange modified the parameters of the exciton Hamiltonian of AmPSI to be closer to the Chl-*a*-containing (native) TePSI rather than to the Chl-*d*-containing (native) AmPSI.

We found that Chl-*a*-containing AmPSI has a distribution of exciton states similar to that of native TePSI, as shown in Figure S4. This is because of the significant changes in the negative site energy shifts and the rescaling of the excitonic coupling strength caused by the pigment exchange from Chl-*d* (with a transition dipole moment of 5.8 Debye) to Chl-*a* (4.8 Debye). The lower exciton states in AmPSI(Chl-*a*) are distributed closer to the main absorption peak because of the smaller absolute value of the negative site energy shift than that of AmPSI. The line absorption spectrum of AmPSI(Chl-*a*) resembles that of TePSI, as shown in Figure S4, because the widths of the stronger excitonic bands are qualitatively proportional to the strengths of the excitonic coupling. Consequently, we found that the electrostatic interactions between pigment charges and protein environments in AmPSI are almost similar to those in TePSI.

Analysis of EET dynamics in AmPSI containing Chl-*a* or Chl-*d*

Transient difference absorption spectra induced by the 630 nm pulse excitation are calculated for AmPSI(Chl-*a*), as shown in Figure 7c. In this analysis, the site energy values of Pheo-*a* was adjusted to yield a peak at 666 nm to fit the experimental spectrum. The 630 nm laser pulse, then, excites Pheo-*a* mainly and induces a fast decrease in absorption at 670 nm. The Chl-*d* to Chl-*a* exchange in AmPSI shifts the peak of the quasi-stationary exciton state to the shorter wavelengths and decreases the exciton band gap by approximately 20 nm (= 400 cm^{-1}). This accelerates exciton relaxation to result in a short transition time. Then, the EET from Pheo-a^* to the exciton states at approximately 690 nm of Chl-*a* occurred faster in less than 0.1 ps. The site energy values in vacuum were used for Chl-*d* ($E_0^{\mathrm{Chl}-d}$ = 700 nm) and Chl-*a* ($E_0^{\mathrm{Chl}-a}$ = 680 nm), so that the different molecular properties of Chl-*a* and Chl-*d* are the main source of this faster downhill EET from the excited Pheo-*a* to the quasi-stationary exciton state in the Chl-*a*-containing AmPSI. Chl-*a* appears to properly bind to the Chl-*d* binding sites in AmPSI judging from the similar site energy shift values (energy required to exchange each Chl-*d* by Chl-*a* in the protein electrostatic environments in AmPSI). This is probably due to the functional and evolutionary close relationship between the protein structures and pigment arrangements between AmPSI and TePSI. It is surprising that the structures of these RCs are optimized to efficiently harvest photon energy, even in different light environments. It shows that the differences between physical properties of Chl-*d* and Chl-*a* alter

the quality of photon absorption with rather small effects on the total EET efficiency.

CONCLUSION

The exciton model for the far-red light adapted AmPSI was constructed using the P-TrESP/CDC methods and the high-resolution structure of AmPSI obtained by cryo-EM analysis.[28] The model enabled an analysis of the light-harvesting mechanism on AmPSI, numerically calculated the experimental absorption/CD spectra of AmPSI, as well as the transient absorption spectra that reflect the excitation energy transfer dynamics. However, it is still a little difficult to reproduce the long wavelength absorption bands around 730 nm correctly by the model. We then evaluated the structures proposed by two recent cryo-EM studies and newly identified 7 Chl-*d*-binding sites did not seem to contribute to the long-wavelength absorption bands at around 730 nm. The electrostatic contribution of α-carotene to the site energy shift of the Chl-*d* molecules in the lower exciton state was also discussed.

The excitonic coupling strength and site energy shift were compared between the theoretical models of AmPSI and TePSI. High correlations between the parameters of the two exciton models are shown. Different distributions of transition ESP charges and difference ESP charges in Chl-*d* and Chl-*a* mainly interpret the stronger exciton coupling strength between Chl-*d* and the larger site energy shifts in each Chl-*d* in AmPSI. It interprets that the simple d-d approximation method provides a more reliable calculation for AmPSI compared to that for TePSI.

We further changed the parameters of Chl-*d* to those of Chl-*a* in the exciton Hamiltonian of AmPSI to perform pigment exchange *in silico*. Then, the virtually produced Chl-*a*-containing AmPSI exhibited physical properties of the exciton Hamiltonian closer to the native Chl-*a*-containing TePSI than to the native Chl-*d*-containing AmPSI. The contribution of the protein moiety of AmPSI to the exciton Hamiltonian is similar to that of TePSI. Therefore, the physical properties of Chl-*d* and Chl-*a* themselves, namely, the *in situ* site energy values in vacuum and the TDM strengths, are found to mainly determine the distribution of the exciton states that control the features of the light-harvesting mechanisms in AmPSI and TePSI.

The study indicates that the electronic feature of Chl-*d* is a key factor for the harvesting of far-red light. The transition dipole strength on Chl-*d* that is stronger than that on Chl-*a* allows the absorption of the far-red light. It also gives the stronger excitonic interaction between the pigments and induces the longer-wavelength exciton bands. The proteins of AmPSI, which are essentially homologous to, but somewhat different from, those of TePSI provide the proper arrangement of Chl-*d* to the locations giving similar site energy shifts distribution, and supports the efficient EET. The reactions of P740, A_0 as well as the output redox powers in AmPSI will be studied elsewhere based on the current model.

We assume that the light-harvesting mechanisms in the RCs have been optimized functionally/evolutionally by the selection of pigments to fit different light environments. We propose that the adaptation of PSI to the far-red light environments was achieved mainly by the introduction/production of Chl-*d*, into the type-I-RC protein environments, which has been optimized evolutionally for the other chlorophylls.

ACKNOWLEDGEMENTS

A.K. acknowledges support from KAKENHI (20K03880). H.K.-N. acknowledge the support from the MEXT Quantum Leap Flagship Program (MEXT Q-LEAP), Grant Number JPMXS0120330644. K.K. acknowledges support from KAKENHI (20H05109). Y.K. acknowledges support from KAKENHI (18H05175). S.I. acknowledges the support from KAKENHI grants

(17K07440 and 20K06684). A part of the computation in this work was performed using the supercomputer of ACCMS, Kyoto University. The authors are grateful to Ms. Yuka Nakamura and Mr. Wataru Shimooka of Nagoya University for their valuable discussion during the study.

Supporting Information Available

Computational details and dataset of the excitonic couplings used in the calculation. Graphical arrangements of the distribution probabilities of the excited state of Chl-*d*, Chl-*d*′, and Pheo-*a* in AmPSI for each exciton state from No. 1 to 73. Dataset of component decomposition of site energy shift ($\epsilon_{\text{eff}} = 1$) of AmPSI.

References

(1) Blankenship, R. E. *Molecular Mechanisms of Photosynthesis, 2nd Edition.*; John Wiley & Sons, Ltd, 2014.

(2) Sener, M. K.; Lu, D.; Ritz, T.; Park, S.; Fromme, P.; Schulten, K. Robustness and Optimality of Light Harvesting in Cyanobacterial Photosystem I. *J. Phys. Chem. B* **2002**, *106*, 7948–7960.

(3) Yang, M.; Damjanović, A.; Vaswani, H. M.; Fleming, G. R. Energy Transfer in Photosystem I of Cyanobacteria *Synechococcus elongatus*: Model Study with Structure-Based Semi-Empirical Hamiltonian and Experimental Spectral Density. *Biophys. J.* **2003**, *85*, 140 – 158.

(4) Heathcote, P.; Jones, M. R.; Fyfe, P. K. Type I Photosynthetic Reaction Centres: Structure and Function. *Phil. Trans. R. Soc. Lond. B* **2003**, *358*, 231–243.

(5) Vaitekonis, S.; Trinkunas, G.; Valkunas, L. Red Chlorophylls in the Exciton Model of Photosystem I. *Photosynth. Res.* **2005**, *86*, 185–201.

(6) Raszewski, G.; Renger, T. Light Harvesting in Photosystem II Core Complexes Is Limited by the Transfer to the Trap: Can the Core Complex Turn into a Photoprotective Mode? *J. Am. Chem. Soc.* **2008**, *130*, 4431–4446.

(7) Abramavicius, D.; Mukamel, S. Exciton Delocalization and Transport in Photosystem I of Cyanobacteria *Synechococcus elongates*: Simulation Study of Coherent Two-Dimensional Optical Signals. *J. Phys. Chem. B* **2009**, *113*, 6097–6108.

(8) Adolphs, J.; Müh, F.; Madjet, M. E.-A.; Busch, M. S. a.; Renger, T. Structure-Based Calculations of Optical Spectra of Photosystem I Suggest an Asymmetric Light-Harvesting Process. *J. Am. Chem. Soc.* **2010**, *132*, 3331–3343.

(9) Shibata, Y.; Yamagishi, A.; Kawamoto, S.; Noji, T.; Itoh, S. Kinetically Distinct Three Red Chlorophylls in Photosystem I of *Thermosynechococcus elongatus* Revealed by Femtosecond Time-Resolved Fluorescence Spectroscopy at 15 K. *J. Phys. Chem. B* **2010**, *114*, 2954–2963.

(10) Shibata, Y.; Nishi, S.; Kawakami, K.; Shen, J.-R.; Renger, T. Photosystem II Does Not Possess a Simple Excitation Energy Funnel: Time-Resolved Fluorescence Spectroscopy Meets Theory. *J. Am. Chem. Soc.* **2013**, *135*, 6903–6914.

(11) Kimura, A.; Itoh, S. Theoretical Model of Exciton States and Ultrafast Energy Transfer in Heliobacterial Type I Homodimeric Reaction Center. *J. Phys. Chem. B* **2018**, *122*, 11852–11859.

(12) Kondo, T.; Matsuoka, M.; Azai, C.; Kobayashi, M.; Itoh, S.; Oh-oka, H. Light-Induced Electron Spin-Polarized (ESP) EPR Signal of the P800+ Menaquinone– Radical Pair State in Oriented Membranes of *Heliobacterium modesticaldum*: Role/Location of Menaquinone in the Homodimeric Type I Reaction Center. *J. Phys. Chem. B* **2018**, *122*, 2536–2543.

(13) Kato, K.; Shinoda, T.; Nagao, R.; Akimoto, S.; Suzuki, T.; Dohmae, N.; Chen, M.; Allakhverdiev, S. I.; Shen, J. R.; Akita, F. et al. Structural Basis for the Adaptation and Function of Chlorophyll *f* in Photosystem I. *Nat. Commun.* **2020**, *11*, 238.

(14) Kojima, R.; Yamamoto, H.; Azai, C.; Uragami, C.; Hashimoto, H.; Kosumi, D.; Oh-oka, H. Energy Transfer and Primary Charge Separation upon Selective Femtosecond Excitation at 810 nm in the Reaction Center Complex from *Heliobacterium modesticaldum*. *J. Photoch. Photobio. A* **2020**, *401*, 112758.

(15) Kondo, T.; Mutoh, R.; Tabe, H.; Kurisu, G.; Oh-Oka, H.; Fujiyoshi, S.; Matsushita, M. Cryogenic Single-Molecule Spectroscopy of the Primary Electron Acceptor in the Photosynthetic Reaction Center. *J. Phys. Chem. Lett.* **2020**, *11*, 3980–3986.

(16) Kitoh-Nishioka, H.; Shigeta, Y.; Itoh, S.; Kimura, A. Excitonic Coupling on a Heliobacterial Symmetrical Type-I Reaction Center: Comparison with Photosystem I. *J. Phys. Chem. B* **2020**, *124*, 389–403.

(17) Kimura, A.; Kitoh-Nishioka, H.; Shigeta, Y.; Itoh, S. Comparison between the Light-Harvesting Mechanisms of Type-I Photosynthetic Reaction Centers of Heliobacteria and Photosystem I: Pigment Site Energy Distribution and Exciton State. *J. Phys. Chem. B* **2021**, *125*, 3727–3738.

(18) Song, Y.; Sechrist, R.; Nguyen, H. H.; Johnson, W.; Abramavicius, D.; Redding, K. E.; Ogilvie, J. P. Excitonic Structure and Charge Separation in the Heliobacterial Reaction Center Probed by Multispectral Multidimensional Spectroscopy. *Nature Commun.* **2021**, *12*, 2801.

(19) Akhtar, P.; Caspy, I.; Nowakowski, P. J.; Malavath, T.; Nelson, N.; Tan, H. S.; Lambrev, P. H. Two-Dimensional Electronic Spectroscopy of a Minimal Photosystem I Complex Reveals the Rate of Primary Charge Separation. *J. Am. Chem. Soc.* **2021**, *143*, 14601–14612.

(20) Jordan, P.; Fromme, P.; Witt, H. T.; Klukas, O.; Saenger, W.; Krauß, N. Three-Dimensional Structure of Cyanobacterial Photosystem I at 2.5 Å Resolution. *Nature* **2001**, *411*, 909–917.

(21) Umena, Y.; Kawakami, K.; Shen, J.-R.; Kamiya, N. Crystal Structure of Oxygen-evolving Photosystem II at a Resolution of 1.9 Å. *Nature* **2011**, *473*, 55–61.

(22) Nelson, N.; Junge, W. Structure and Energy Transfer in Photosystems of Oxygenic Photosynthesis. *Annu. Rev. Biochem.* **2015**, *84*, 659–683.

(23) Miyashita, H.; Ikemoto, H.; Kurano, N.; Adachi, K.; Chihara, M.; Miyachi, S. Chlorophyll *d* as a Major Pigment. *Nature* **1996**, *383*, 402.

(24) Hu, Q.; Miyashita, H.; Iwasaki, I.; Kurano, N.; Miyachi, S.; Iwaki, M.; Itoh, S. A Photosystem I Reaction Center Driven by Chlorophyll *d* in Oxygenic Photosynthesis. *Proc. Natl. Acad. Sci. USA* **1998**, *95*, 13319–13323.

(25) Ohashi, S.; Miyashita, H.; Okada, N.; Iemura, T.; Watanabe, T.; Kobayashi, M. Unique Photosystems in *Acaryochloris marina*. *Photosynth. Res.* **2008**, *98*, 141–149.

(26) Itoh, S.; Mino, H.; Itoh, K.; Shigenaga, T.; Uzumaki, T.; Iwaki, M. Function of Chlorophyll *d* in Reaction Centers of Photosystems I and II of the Oxygenic Photosynthesis of *Acaryochloris marina*. *Biochemistry* **2007**, *46*, 12472–12481.

(27) Tomo, T.; Kato, Y.; Suzuki, T.; Akimoto, S.; Okubo, T.; Noguchi, T.; Hasegawa, K.; Tsuchiya, T.; Tanaka, K.; Fukuya, M. et al. Characterization of Highly Purified Photosystem I Complexes from the Chlorophyll *d*-Dominated Cyanobacterium *Acaryochloris marina* MBIC 11017. *J. Biol. Chem.* **2008**, *283*, 18198–18209.

(28) Hamaguchi, T.; Kawakami, K.; Shinzawa-Itoh, K.; Inoue-Kashino, N.; Itoh, S.; Ifuku, K.; Yamashita, E.; Maeda, K.; Yonekura, K.; Kashino, Y. Structure of the Far-Red Light Utilizing Photosystem I of *Acaryochloris marina*. *Nat. Commun.* **2021**, *12*, 2333.

(29) Mazor, Y.; Borovikova, A.; Nelson, N. The Structure of Plant Photosystem I Super-Complex at 2.8 Å Resolution. *eLife* **2015**, *4*, e07433.

(30) Qin, X.; Suga, M.; Kuang, T.; Shen, J.-R. Structural Basis for Energy Transfer Pathways in the Plant PSI-LHCI Supercomplex. *Science* **2015**, *348*, 989–995.

(31) Qin, X.; Pi, X.; Wang, W.; Han, G.; Zhu, L.; Liu, M.; Cheng, L.; Shen, J. R.; Kuang, T.; Sui, S. F. Structure of a Green Algal Photosystem I in Complex with a Large Number of Light-Harvesting Complex I Subunits. *Nat. Plants* **2019**, *5*, 263–272.

(32) Suga, M.; Ozawa, S. I.; Yoshida-Motomura, K.; Akita, F.; Miyazaki, N.; Takahashi, Y. Structure of the Green Algal Photosystem I Supercomplex with a Decameric Light-Harvesting Complex I. *Nat. Plants* **2019**, *5*, 626–636.

(33) Pi, X.; Tian, L.; Dai, H. E.; Qin, X.; Cheng, L.; Kuang, T.; Sui, S. F.; Shen, J. R. Unique Organization of Photosystem I–Light-Harvesting Supercomplex Revealed by Cryo-EM from a Red Alga. *Proc. Natl. Acad. Sci. USA* **2018**, *115*, 4423–4428.

(34) Nagao, R.; Kato, K.; Ifuku, K.; Suzuki, T.; Kumazawa, M.; Uchiyama, I.; Kashino, Y.; Dohmae, N.; Akimoto, S.; Shen, J.-R. et al. Structural Basis for Assembly and Function of a Diatom Photosystem I-Light-Harvesting Supercomplex. *Nat. Commun.* **2020**, *11*, 2481.

(35) Nürnberg, D. J.; Morton, J.; Santabarbara, S.; Telfer, A.; Joliot, P.; Antonaru, L. A.; Ruban, A. V.; Cardona, T.; Krausz, E.; Boussac, A. et al. Photochemistry Beyond the Red Limit in Chlorophyll *f*–Containing Photosystems. *Science* **2018**, *360*, 1210–1213.

(36) Gisriel, C.; Shen, G.; Kurashov, V.; Ho, M. Y.; Zhang, S.; Williams, D.; Golbeck, J. H.; Fromme, P.; Bryant, D. A. The Structure of Photosystem I Acclimated to Far-Red Light Illuminates an Ecologically Important Acclimation Process in Photosynthesis. *Sci. Adv.* **2020**, *6*, eaay6415.

(37) Gisriel, C. J.; Wang, J.; Brudvig, G. W.; Bryant, D. A. Opportunities and Challenges for Assigning Cofactors in Cryo-EM Density Maps of Chlorophyll-Containing Proteins. *Commun. Biol.* **2020**, *3*, 403.

(38) Kato, K.; Nagao, R.; Jiang, T. Y.; Ueno, Y.; Yokono, M.; Chan, S. K.; Watanabe, M.; Ikeuchi, M.; Shen, J. R.; Akimoto, S. et al. Structure of a Cyanobacterial Photosystem I Tetramer Revealed by Cryo-Electron Microscopy. *Nat. Commun.* **2019**, *10*, 4929.

(39) Malavath, T.; Caspy, I.; Netzer-El, S. Y.; Klaiman, D.; Nelson, N. Structure and Function of Wild-Type and Subunit-Depleted Photosystem I in *Synechocystis*. *Biochim. Biophys. Acta Bioenerg.* **2018**, *1859*, 645–654.

(40) Gisriel, C. J.; Shen, G.; Ho, M.-Y.; Kurashov, V.; Flesher, D. A.; Wang, J.; Armstrong, W. H.; Golbeck, J. H.; Gunner, M. R.; Vinyard, D. J. et al. Structure of a Monomeric Photosystem II Core Complex from a Cyanobacterium Acclimated to Far-Red Light Reveals the Functions of Chlorophylls *d* and *f*. *J. Biol. Chem.* **2022**, *298*, 101424.

(41) Gisriel, C.; Sarrou, I.; Ferlez, B.; Golbeck, J. H.; Redding, K. E.; Fromme, R. Structure of a Symmetric Photosynthetic Reaction Center–Photosystem. *Science* **2017**, *357*, 1021–1025.

(42) Chen, J.-H.; Wu, H.; Xu, C.; Liu, X.-C.; Huang, Z.; Chang, S.; Wang, W.; Han, G.; Kuang, T.; Shen, J.-R. et al. Architecture of the Photosynthetic Complex from a Green Sulfur Bacterium. *Science* **2020**, *370*, eabb6350.

(43) Bailleul, B.; Johnson, X.; Finazzi, G.; Barber, J.; Rappaport, F.; Telfer, A. The Thermodynamics and Kinetics of Electron Transfer between Cytochrome b_6f and Photosystem I in the Chlorophyll *d*-Dominated Cyanobacterium, *Acaryochloris marina*. *J. Biol. Chem.* **2008**, *283*, 25218–25226.

(44) Chen, M.; Schliep, M.; Willows, R. D.; Cai, Z.-L.; Neilan, B. A.; Scheer, H. A Red-Shifted Chlorophyll. *Science* **2010**, *329*, 1318–1319.

(45) Gan, F.; Zhang, S.; Rockwell, N. C.; Martin, S. S.; Lagarias, J. C.; Bryant, D. A. Extensive Remodeling of a Cyanobacterial Photosynthetic Apparatus in Far-Red Light. *Science* **2014**, *345*, 1312–1317.

(46) Miyashita, H.; Ohkubo, S.; Komatsu, H.; Sorimachi, Y.; Fukayama, D.; Fujinuma, D.; Akutsu, S.; Kobayashi, M. Discovery of Chlorophyll *d* in *Acaryochloris marina* and Chlorophyll *f* in a Unicellular Cyanobacterium, Strain KC1, Isolated from Lake Biwa. *J. Phys. Chem. Biophys.* **2014**, *4*, 1000149.

(47) Kaucikas, M.; Nürnberg, D.; Dorlhiac, G.; Rutherford, A. W.; van Thor, J. J. Femtosecond Visible Transient Absorption Spectroscopy of Chlorophyll *f*-Containing Photosystem I. *Biophys. J.* **2017**, *112*, 234–249.

(48) Kurashov, V.; Ho, M. Y.; Shen, G.; Piedl, K.; Laremore, T. N.; Bryant, D. A.; Golbeck, J. H. Energy Transfer from Chlorophyll *f* to the Trapping Center in Naturally Occurring and Engineered Photosystem I Complexes. *Photosynth. Res.* **2019**, *141*, 151–163.

(49) Cherepanov, D. A.; Shelaev, I. V.; Gostev, F. E.; Aybush, A. V.; Mamedov, M. D.; Shen, G.; Nadtochenko, V. A.; Bryant, D. A.; Semenov, A. Y.; Golbeck, J. H. Evidence That Chlorophyll *f* Functions Solely as an Antenna Pigment in Far-Red-Light Photosystem I from *Fischerella thermalis* PCC 7521. *Biochim. Biophys. Acta Bioenerg.* **2020**, *1861*, 148184.

(50) Judd, M.; Morton, J.; Nürnberg, D.; Fantuzzi, A.; Rutherford, A. W.; Purchase, R.; Cox, N.; Krausz, E. The Primary Donor of Far-Red Photosystem II: ChlD1 or PD2? *Biochim. Biophys. Acta Bioenerg.* **2020**, *1861*, 148248.

(51) Schmitt, F. J.; Campbell, Z. Y.; Bui, M. V.; Hüls, A.; Tomo, T.; Chen, M.; Maksimov, E. G.; Allakhverdiev, S. I.; Friedrich, T. Photosynthesis Supported by a Chlorophyll *f*-Dependent, Entropy-Driven Uphill Energy Transfer in *Halomicronema hongdechloris* Cells Adapted to Far-Red Light. *Photosynth. Res.* **2019**, *139*, 185–201.

(52) Toporik, H.; Khmelnitskiy, A.; Dobson, Z.; Riddle, R.; Williams, D.; Lin, S.; Jankowiak, R.; Mazor, Y. The Structure of a Red-Shifted Photosystem I Reveals a Red Site in the Core Antenna. *Nat. Commun.* **2020**, *11*, 5279.

(53) Xu, C.; Zhu, Q.; Chen, J.-H.; Shen, L.; Yi, X.; Huang, Z.; Wang, W.; Chen, M.; Kuang, T.; Shen, J.-R. et al. A Unique Photosystem I Reaction Center from a Chlorophyll *d*-Containing Cyanobacterium *Acaryochloris marina*. *J. Integr. Plant Biol.* **2021**, *63*, 1740–1752.

(54) Kumazaki, S.; Abiko, K.; Ikegami, I.; Iwaki, M.; Itoh, S. Energy Equilibration and Primary Charge Separation in Chlorophyll *d*-Based Photosystem I Reaction Center Isolated from *Acaryochloris marina*. *FEBS Lett.* **2002**, *530*, 153–157.

(55) Mi, D.; Chen, M.; Lin, S.; Lince, M.; Larkum, A. W.; Blankenship, R. E. Excitation Dynamics in the Core Antenna in the Photosystem I Reaction Center of the Chlorophyll *d*-Containing Photosynthetic Prokaryote *Acaryochloris marina*. *J. Phys. Chem. B* **2003**, *107*, 1452–1457.

(56) Renger, T.; Müh, F. Theory of Excitonic Couplings in Dielectric Media. Foundation of Poisson-TrEsp Method and Application to Photosystem I Trimers. *Photosynth. Res.* **2012**, *111*, 47–52.

(57) Yanai, T.; Tew, D. P.; Handy, N. C. A New Hybrid Exchange-Correlation Functional Using the Coulomb-Attenuating Method (CAM-B3LYP). *Chem. Phys. Lett.* **2004**, *393*, 51 – 57.

(58) Schmidt, M. W.; Baldridge, K. K.; Boatz, J. A.; Elbert, S. T.; Gordon, M. S.; Jensen, J. H.; Koseki, S.; Matsunaga, N.; Nguyen, K. A.; Su, S. et al. General Atomic and Molecular Electronic Structure System. *J. Comput. Chem.* **1993**, *14*, 1347–1363.

(59) Knox, R. S.; Spring, B. Q. Dipole Strengths in the Chlorophylls. *Photochem. Photobiol.* **2003**, *77*, 497–501.

(60) Pessarakli, M. E. *Handbook of Photosynthesis, Third Edition. Boca Raton*; CRC Press., 2016.

(61) Baker, N. A.; Sept, D.; Joseph, S.; Holst, M. J.; McCammon, J. A. Electrostatics of Nanosystems: Application to Microtubules and the Ribosome. *Proc. Natl. Acad. Sci. USA* **2001**, *98*, 10037–10041.

(62) Saito, K.; Suzuki, T.; Ishikita, H. Absorption-Energy Calculations of Chlorophyll *a* and *b* with an Explicit Solvent Model. *J. Photochem. Photobiol. A* **2018**, *358*, 422–431.

(63) Shao, Y.; Gan, Z.; Epifanovsky, E.; Gilbert, A. T.; Wormit, M.; Kussmann, J.; Lange, A. W.; Behn, A.; Deng, J.; Feng, X. et al. Advances in Molecular Quantum Chemistry Contained in the Q-Chem 4 Program Package. *Mol. Phys.* **2015**, *113*, 184–215.

(64) Maier, J. A.; Martinez, C.; Kasavajhala, K.; Wickstrom, L.; Hauser, K. E.; Simmerling, C. ff14SB: Improving the Accuracy of Protein Side Chain and Backbone Parameters from ff99SB. *J. Chem. Theory Comput.* **2015**, *11*, 3696–3713.

(65) Redfield, A. G. On the Theory of Relaxation Processes. *IBM J. Res. Dev.* **1957**, *1*, 19.

(66) Renger, T.; Marcus, R. A. On the Relation of Protein Dynamics and Exciton Relaxation in Pigment–Protein Complexes: An Estimation of the Spectral Density and a Theory for the Calculation of Optical Spectra. *J. Chem. Phys.* **2002**, *116*, 9997–10019.

(67) Aota, T. Cryogenic Laser Photolysis of Photosystem I Reaction Center of *Acaryochloris marina* (in Japanese). M.Sc. thesis, Grad. Sch. Sci, Nagoya Univ., Nagoya, Japan, 2009.

Graphical TOC Entry